Fitting Parameter Estimations for Droplet Breakage Rate Models

Krishnamurthy Ravichandar[a], R. Dennis Vigil[b], Michael G. Olsen[a,*]

[a]*Department of Mechanical Engineering Iowa State University Ames IA 50011*
[b]*Department of Chemical and Biological Engineering Iowa State University Ames IA 50011*

Abstract

Chemical process engineering unit operations such as solvent extraction, liquid-liquid chemical reactions, and emulsion processing are all dependent on turbulent liquid-liquid droplet flow dynamics. The design and operation of equipment used in these applications is often guided by theoretical models for droplet breakup. Although several models for droplet breakage in agitated liquid emulsions have been developed, their utility is limited because they incorporate fitting factors that must be determined empirically by performing experiments using a specific fluid pairing and relevant flow configuration. The need to acquire experimental data to determine model constants is a significant drawback that hinders widespread use of breakage models to design and optimize process equipment. In this work, analytical expressions are formulated to predict the value of a fitting parameter associated with droplet breakage time for two commonly used breakage rate models without having to perform empirical studies. These equations were derived by using the underlying assumptions within each of the two breakage models considered, namely that droplet breakage is a result of the competition between relevant deformation and restorative stresses. Data from experiments conducted in a homogeneous turbulent von Kármán box as well as from previously published investigations of droplet breakage in heterogeneous flow devices were utilized to validate the derived equations for the breakage time parameters. In general, good agreement was observed between predictions obtained using the derived equations for fitting parameters and those obtained from experiments.

Preprint submitted to Physics of Fluids *November 15, 2023*

1. Introduction

Dispersion of one immiscible liquid in another plays an important role in many chemical manufacturing unit operations, such as extraction and liquid-liquid reactions. Liquid emulsions are also produced during manufacture of a wide variety of products including food, pharmaceuticals([1–3]), and cosmetics ([4, 5]), and they play an important role in oil production and environmental remediation technology. The properties and behavior of a liquid emulsion are closely tied to the dispersed phase droplet size distribution, which in turn depends upon the method for generating the emulsion. Liquid dispersions are commonly produced and sustained using mechanical agitation to generate turbulent stresses sufficient to cause droplet breakage and to create large interfacial area. Consequently, the design, operation, and scaleup of equipment used to process emulsions requires development of validated models that accurately describe the physical phenomena that govern droplet dynamics in turbulent flow, such as drop coagulation and breakage.

The understanding of droplet breakage in turbulent flows has been a subject of extensive research, with various models and approaches proposed to elucidate the breakage time, probability, and rate of droplets in such flows. presented a model for the breakage rate of drops in turbulent flow, considering the product of certain parameters. contributed to the understanding of droplet breakage in turbulent flows, focusing on the evolution of particle size distribution. Additionally, proposed a population balance model for the prediction of breakage of emulsion droplets. predicted droplet size distribution, breakage frequency, and coalescence rate using a CFD-PBM investigation. These studies collectively provide valuable insights into the mechanisms and factors influencing droplet breakage in turbulent flows.

The influence of turbulence on droplet breakage has been a focus of research. highlighted that droplet breakage occurs mostly in the dissipation range of isotropic turbulence, empha-

*Corresponding author
URL: mgolsen@iastate.edu (Michael G. Olsen)

sizing the role of turbulent energy in the breakage process. Various models and approaches have been proposed to understand the breakage time, probability, and rate of droplets in turbulent flow. Tsouris & Tavlarides [6] proposed a model for the breakage rate of drops in turbulent flow, considering the product of certain parameters. Kostoglou [7] and Lebaz & Sheibat-Othman [8] also contributed to the understanding of droplet breakage in turbulent flows, considering the evolution of particle size distribution and proposing a population balance model for the prediction of breakage of emulsion droplets, respectively. Additionally, Tan et al. [9] predicted droplet size distribution, breakage frequency, and coalescence rate using a CFD-PBM investigation. These studies provide valuable insights into the mechanisms and factors influencing droplet breakage in turbulent flows.

In addition to the aforementioned studies, further research by Herø et al.[1] presented a theoretical model for drop and bubble breakup in turbulent dispersions, supported by experimental results for bubble and drop breakage in turbulent pipe flows. Castellano et al. [10] focused on the breakup of an air bubble injected into fully developed turbulent flow, emphasizing the breakup frequency. Furthermore, Forgia et al.[1] Luo & Svendsen [11] made an important contribution to the modeling of dispersed phase distribution in multiphase flow, establishing the foundation for models of droplet breakage and coalescence in turbulent flow for use with Population Balance Equation (PBE). These additional studies further enrich the understanding of droplet breakage in turbulent flows, providing insights into breakup frequency, dispersion modeling, and the theoretical aspects of droplet breakup.

Although numerous models have been proposed to describe drop breakage in turbulent liquid emulsions, these models include fitting parameters that must be determined empirically for a specific set of fluid physical properties and operating conditions [12]. Furthermore, most models incorporate turbulence parameters that may vary greatly with position in the flow apparatus, as is the case with stirred tanks. Consequently, fitting of breakage parameters in heterogeneous turbulent flows is usually performed by using volume-averaged values

for model variables such as turbulence dissipation rate, and such approximations can potentially lead to significant errors. To minimize the impact of turbulence heterogeneity on fitted breakage model parameters, the authors recently carried out droplet breakage studies in a von Kármán box [13, 14]. This apparatus generates homogneous turbulence in a large imaging volume surrounding an injection needle that is used to introduce droplets one at a time into the flow. Using dimensional analysis as well as data obtained from the von Kármán box experiments, they also derived and partially validated analytical equations for some fitting parameters associated with breakage models derived by Coulaloglou and Tavlarides (C-T) and by Chen [15]. The work presented here describes the development of analytical expressions for the remaining fitting constants (associated with the characteristic drop breakage time) of the C-T and Chen rate models. These equations are then validated by comparing their predictions with experimental droplet breakage rate data acquired from two sources including (1) experiments performed by the authors in a von Kármán box and (2) previously published reports of droplet breakage in channel flows.

2. Breakage Time Parameters

A continuity equation describing the temporal evolution of the volume distribution of a population of incompressible droplets undergoing breakage in a batch reactor can be expressed in continuous form as

$$\frac{\partial c(v,t)}{\partial t} = -a(v)c(v,t) + \int_v^\infty a(u)b(v|u)c(u,t)du \tag{1}$$

In the above expression, c(v,t) is the number concentration of droplets with volume v at time t. The first term on the right side of Eq.(1) represents the rate of breakage of droplets with volume v, where a(v) is the size-dependent rate coefficient having units of inverse time. The integral term represents the rate of formation of droplets with volume v due to breakage

of larger droplets. Calculation of the latter term requires knowledge of the probability that a droplet of volume v is produced from the breakage of a droplet of volume u, where $u > v$. This information is provided by the conditional child distribution function, $b(v|u)$, which must satisfy continuity (i.e. the masses of the child droplets must sum to the mass of the parent droplet). Note that in this formulation of the breakage equation, multiple child droplets can be produced from a single breakage event.

2.1. Coulaloglou-Tavlarides Model

Although the specific form of the child distribution function can impact the shape of the droplet size distribution $c(v,t)$, the functional form of the breakage rate coefficient $a(v)$ plays the most significant role in determining the evolution of systems undergoing droplet breakage. One of the earliest and most widely-adopted expressions for the breakage rate coefficient was proposed by Coulaloglou and Tavlarides, who used an energy-based analysis that assumes droplet breakage (or lack thereof) is determined by competition between turbulent and interfacial stresses [16]. The resulting breakage rate coefficient, when expressed using drop diameter rather than volume as the internal coordinate (assuming that droplets are spherical), is given by:

$$a(d) = C_1 \varepsilon^{1/3} d^{-2/3} \exp\Big[-\frac{C_2 \sigma}{\rho_d \varepsilon^{2/3} d^{5/3}}\Big], \tag{2}$$

where ε is the turbulence dissipation rate, d is the droplet diameter, ρ_d represents the mass density of the droplets, σ is the liquid-liquid interfacial tension, and C_1 and C_2 are fitting constants assumed to depend in general upon physical properties. The exponential term in Eq. (2) can be associated with the breakage probability of a droplet of diameter d. Previously [13], the authors hypothesized that C_2 can be determined without need for experiments by associating a droplet breakage probability of 50% with the situation in which the disruptive turbulent stress is exactly balanced by the cohesive interfacial stress, and this assumption

leads to the following expression:

$$C_2 = \frac{\rho_d}{2\rho_c} \ln(2), \tag{3}$$

where ρ_c is the density of the continuous fluid. The accuracy of Eq. (3) was demonstrated by comparing its predictions with experimental data gathered for droplet breakage probability from multiple investigators. Hence, a one-parameter version of the C-T model can be obtained by substituting Eq. (3) into (2), which leads to

$$a(d) = C_1 \varepsilon^{1/3} d^{-2/3} \left(\frac{1}{2}\right)^{1/\mathrm{We}}, \tag{4}$$

where the Weber number is defined as

$$\mathrm{We} = \frac{\tau_d}{\tau_\sigma} = \frac{2\rho_c \varepsilon^{2/3} d^{5/3}}{\sigma}. \tag{5}$$

In Eq. (5), τ_d is the disruptive turbulent deformation stress on the droplet and τ_σ is the cohesive interfacial stress, and these are given by:

$$\tau_d = 2\rho_c (\varepsilon d)^{2/3}, \tag{6}$$

$$\tau_\sigma = \tfrac{\sigma}{d}, \tag{7}$$

where σ is the interfacial tension between the droplet and continuous phase [3, 17, 18].

The pre-exponential term in Eq.(2) is a breakage frequency factor with units of inverse time. Hence the C-T model assumes that the characteristic droplet breakage time (t_b) is given by

$$t_b = \tfrac{1}{C_1} \varepsilon^{-1/3} d^{2/3} \tag{8}$$

The right side of Eq. (8) is proportional to the eddy turnover time at length scale d. However, for cases in which the internal viscous force can be neglected, (which is an implicit assumption of the C-T model), the droplet deformation time not only depends on the turbulent deformation stress, but it also is influenced by the inertial resistance to deformation in the interior fluid. Consequently, the characteristic droplet breakage time should incorporate the densities of the internal (ρ_d)and external (ρ_c) fluids according to the following expression [19]:

$$t_b = \frac{1}{C_1}\frac{d^{2/3}}{\varepsilon^{1/3}}\sqrt{\frac{\rho_d}{\rho_c}}. \tag{9}$$

Equation (9) can be expressed in dimensionless form by dividing breakage time, t_b, by the Kolomogrov time scale $t_\eta = \sqrt{\nu_c/\varepsilon}$, which leads to:

$$t_b^* = \frac{t_b}{\sqrt{\nu_c/\varepsilon}} = \frac{\rho_c}{C_1}\left(\frac{\sigma d}{2\rho_c}\right)^{1/4}\left(\frac{1}{\mu_c\rho_d}\right)^{1/2}\mathrm{We}^{1/4} \tag{10}$$

where ν_c is the kinematic viscosity of the continuous phase. Equation (10) can be expressed more succintly by making use of the Ohnesorge number, Oh, defined as:

$$\mathrm{Oh} = \frac{\mu_{\mathbf{c}}}{\sqrt{\rho_{\mathbf{c}}\sigma d}}, \tag{11}$$

where μ_c is the dynamic viscosity of the continuous phase. Combining Eqs. (10) and (11) leads to

$$t_b^* = \frac{2^{\frac{1}{4}}}{C_1}\sqrt{\frac{\rho_d}{\rho_c}}\mathrm{Oh}^{-1/2}\mathrm{We}^{1/4}. \tag{12}$$

Although Eqn. (12) seems to imply that breakage time increases with increasing turbulence dissipation rate, in fact the opposite is true since t_b^* is directly proportional to ε whereas $\mathrm{We}^{1/4} \sim \varepsilon^{1/6}$.

Since the dependence of breakage time on ε and d is already accounted for explicitly in the formulation of Eq. (9) via the characteristic eddy turnover time, it could be expected

that C_1 has a value of order unity. Such an approximation is consistent with the assumption that C_1 is chosen so that

$$C_1 = \mathrm{We}_{cr} \tag{13}$$

where We_{cr} is a unique Weber number with a specific physical meaning. Here we hypothesize that an appropriate choice for We_{cr} is obtained by considering the case in which the disruptive and restorative stresses are equal:

$$\tau_d = \tau_\sigma. \tag{14}$$

If follows from Eqs. (5), and (14) that

$$\mathrm{We}_{cr} = 1. \tag{15}$$

Hence, for instances in which the C-T model is applicable (breakage is determined primarily by τ_d and τ_σ), we hypothesize that $C_1 = \mathrm{We}_{cr} = 1$, and therefore Eq. (9) can be expressed as:

$$t_b^* = 2^{\frac{1}{4}} \sqrt{\frac{\rho_d}{\rho_c}} \mathrm{Oh}^{-1/2} \mathrm{We}^{1/4}. \tag{16}$$

without need for determining fitting parameters empirically. Combining Eqs. (4) and (16) leads to the following expression for the dimensionless breakage rate, $a^*(d)$:

$$a^*(d) = a(d) \sqrt{\frac{\nu_c}{\varepsilon}} = 2^{-1/4} \sqrt{\frac{\rho_c}{\rho_d}} \mathrm{Oh}^{1/2} \mathrm{We}^{-1/4} \left(\frac{1}{2}\right)^{1/\mathrm{We}}. \tag{17}$$

The predictions of Eqs. (16) and (17) are compared with experimental data for breakage time and breakage rate in section 3.1.

2.2. Modified Chen Model

When the internal fluid viscosity is large, the assumption that droplet breakage is primarily a result of competition between turbulent deformation and interfacial stresses is not valid. In such instances, the internal viscous stress, τ_μ, given by [17]:

$$\tau_\mu = \frac{\mu_d}{d}(\varepsilon d)^{1/3}\sqrt{\frac{2\rho_c}{\rho_d}}, \tag{18}$$

contributes a significant portion of the overall stress resisting breakage. Chen *et al.* [15], modified the C-T model by including internal viscous stress in the analysis of breakage probability and also by assuming that droplet breakage time is constant so that

$$a(d) = C_1 \exp\Big[-\frac{C_2\sigma}{\rho_d\varepsilon^{2/3}d^{5/3}}\Big]\exp\Big[-\frac{C_3\mu_d}{\rho_d\varepsilon^{1/3}d^{4/3}}\Big] \tag{19}$$

The second exponential term arises from the viscous stress and reduces droplet breakage probability, as can be seen by comparing Eqs. (2) and (19). Previously [13], the authors showed that C_2 could be determined without the need for prior experiments by associating a droplet breakage probability of 50% with the situation in which the disruptive turbulent stress is exactly balanced by the cohesive interfacial and viscous stress, thereby leading to

$$C_3 = C_2\sqrt{\frac{2\rho_c}{\rho_d}}. \tag{20}$$

In contrast to the assumption of Chen *et al.* that breakage time is constant, it is assumed here that breakage time is given by Eq. (9), and therefore that the breakage rate coefficient is given by

$$a(d) = C_1\varepsilon^{1/3}d^{-2/3}\exp\Big[-\frac{C_2\sigma}{\rho_d\varepsilon^{2/3}d^{5/3}}\Big]\exp\Big[-\frac{C_3\mu_d}{\rho_d\varepsilon^{1/3}d^{4/3}}\Big]. \tag{21}$$

Making use of Eqs. (3) and (20) to eliminate the fitting contants C_2 and C_3 leads to

$$a(d) = C_1 \varepsilon^{1/3} d^{-2/3} \left(\frac{1}{2}\right)^{(1+\mathrm{Ca})/\mathrm{We}}. \tag{22}$$

where Ca is the capillary number defined as [3]:

$$\mathrm{Ca} = \frac{\mu_d}{\sigma}(\varepsilon d)^{1/3}\sqrt{\frac{2\rho_c}{\rho_d}}. \tag{23}$$

In order to eliminate the fitting parameter C_1, which represents a correction to the eddy turnover time on the right side of Eq. (9), we hypothesize that C_1 is given by a characteristic value of the capillary number, Ca_{cr}. Note that the definition of Ca above includes factors present in the turbulent deformation stress, τ_d, the interfacial stress, τ_σ, and the internal viscous stress, τ_μ. A characteristic value of Ca_{cr} can be obtained by equating the disruptive and cohesive stresses so that:

$$\tau_\sigma + \tau_\mu = \tau_d \tag{24}$$

Substituting Eqs. (6), (7), and (18) into Eq. (24) leads to

$$\frac{\sigma}{d_{50}} + \frac{\mu_d}{d_{50}}(\varepsilon d_{50})^{1/3}\sqrt{\frac{2\rho_c}{\rho_d}} = 2\rho_c(\varepsilon d_{50})^{2/3}, \tag{25}$$

where d_{50} denotes the droplet diameter for which the disruptive and cohesive stresses are balanced so that the probability of breakage is approximately 50% [20]. Hence, Eq. (25) can be used to evaluate a critical capillary number defined as

$$Ca_{cr} = \frac{\mu_d}{\sigma}(\varepsilon d_{50})^{1/3}\sqrt{\frac{2\rho_c}{\rho_d}}. \tag{26}$$

We hypothesize that $C_1 = \mathrm{Ca}_{cr}$ and consequently the dimensionless breakage time can be

computed as

$$t_b^* = \frac{2^{\frac{1}{4}}}{Ca_{cr}} \sqrt{\frac{\rho_d}{\rho_c}} \mathrm{Oh}^{-1/2} \mathrm{We}^{1/4}. \tag{27}$$

Combining Eqs. (22) and (27) leads to the following equation for the dimensionless breakage rate, $a^*(d)$:

$$a^*(d) = a(d) \sqrt{\frac{\nu_c}{\varepsilon}} = 2^{-1/4} \mathrm{Ca}_{cr} \sqrt{\frac{\rho_c}{\rho_d}} \mathrm{Oh}^{1/2} \mathrm{We}^{-1/4} \left(\frac{1}{2}\right)^{(1+\mathrm{Ca})/\mathrm{We}}. \tag{28}$$

The predictions of Eqs. (27) and (28) are compared with experimental data for breakage time and breakage rate in section 4.3.

3. Validation of Breakage Model Parameter Predictions

Validation of mathematical models of droplet breakage are hindered by the difficulties associated with acquiring detailed and statistically significant experimental data sets for breakage events carried out under well-controlled conditions. For example, droplet breakage experiments are best performed in a homogeneous flow field, because breakage depends sensitively on the hydrodynamic environment. However, many previous experimental investigations of droplet breakage time in turbulent flows were performed using flow devices, such as channel sections, which are known to produce heterogeneous turbulence. Here, these previously published data sets are supplemented with data collected in a von Kármán box [14] to test the fitting parameter expressions for breakage time and breakage rate developed in the previous section.

3.1. Evaluation of Zero-Parameter Coulaloglou-Tavlarides Model

Droplet breakage time measurements have been reported for experimental studies carried out in channel sections and in stirred tanks [1, 21, 22]. In these previous investigations,

droplet breakage time was determined for various parent droplet sizes and by using a large ensemble of observed breakage events. The authors of these investigations used organic droplet phases paired with water as the continuous phase, and the relevant droplet phase physical properties and estimated turbulence dissipation rates are listed in Table 1. This

Table 1: Organic droplet properties in water and operating parameters reported in droplet breakage studies for toluene, petroleum [21] and n-dodecane-water emulsions [22].

Droplet Phase	ρ **(kg/m^3)**	σ **(N/m)**	μ **(mPa·s)**	ε **(m^2/s^3)**	**We**	**Ca**
Toulene	870	0.032	0.55	5.19	1.9 - 37.1	0.005–0.008
Petroleum	790	0.0385	0.65	5.95	1.7 - 33.8	0.005–0.009
n-Dodecane	750.1	0.03461	1.64	1.20	0.087-1.896	0.0055-0.010
				1.90	0.119-1.369	0.0064-0.011
				3.69	0.185-2.704	0.0079-0.013
2 vol % TBP/n-dodecane	754	0.01958	1.64	1.20	0.155-2.785	0.009-0.017
10 vol % TBP/n-dodecane	778	0.01167	1.65	1.20	0.259-1.929	0.016-0.024

information can be used in conjunction with water physical property data and parent droplet diameters to determine corresponding ranges of values for We and Ca, also shown in Table 1. In all cases the capillary numbers investigated are well below 0.1, thereby suggesting that the classic C-T model, which neglects internal viscous stress, may be appropriate for predicting droplet breakage for these fluid pairs.

Fitted values for the dimensionless breakage time constant C_1 can be obtained from experimental data by using Eq. (9). In order to test the hypothesis that $C_1 = \mathrm{We}_{cr} = 1$, dimensionless breakage time predictions and experimental data are plotted in Figure 1. The range of fitted values for C_1 is listed in Table 2, and the upper and lower bounds were computed using the standard error of the experimental data. For all cases listed in Table 2, the values for C_1 predicted by Eqn. (16) differ from the median value of C_1 of the regressed fits to experimental data by a mean difference of only 6.14%. Thus, Eqn. (16) generally provides a good estimate of breakage time, at least for the fluid pairs tested, without the need for a fitting constant. However, dodecane breakage times are not well predicted by Eq. (16) at the highest values of interfacial tension and turbulence dissipation rate investigated. This mismatch may be accounted for by the fact that the equipment

used to collect the experimental data for these cases produces heterogeneous turbulence, and therefore the reported estimates for the mean turbulence dissipation rates may not be representative of conditions responsible for all of the observed droplet breakage events.

Table 2: Comparison of C_1 values obtained from predictions of Eqs. (16) with values obtained by regressing Eq. (9) to experimental data.

Test Fluid	C_1,**q.**(27)	C_1, **Regressed Average Fit**	C_1, **Regressed Lower Bound**	C_1,**Regressed Upper Bound**	**Percentage Error,Average Fit**
Toulene	1	1.007	0.9829	1.068	0.7
Petroleum	1	1.081	0.7658	1.155	7.49
n-Dodecane	1	1.065	0.7678	1.885	6.1
	1	0.992	0.7865	1.226	0.8
	1	0.876	0.554	1.154	14.15
2 vol % TBP/n-dodecane	1	1.021	0.7606	1.984	2.05
10 vol % TBP/n-dodecane	1	0.8946	0.5212	1.848	11.7

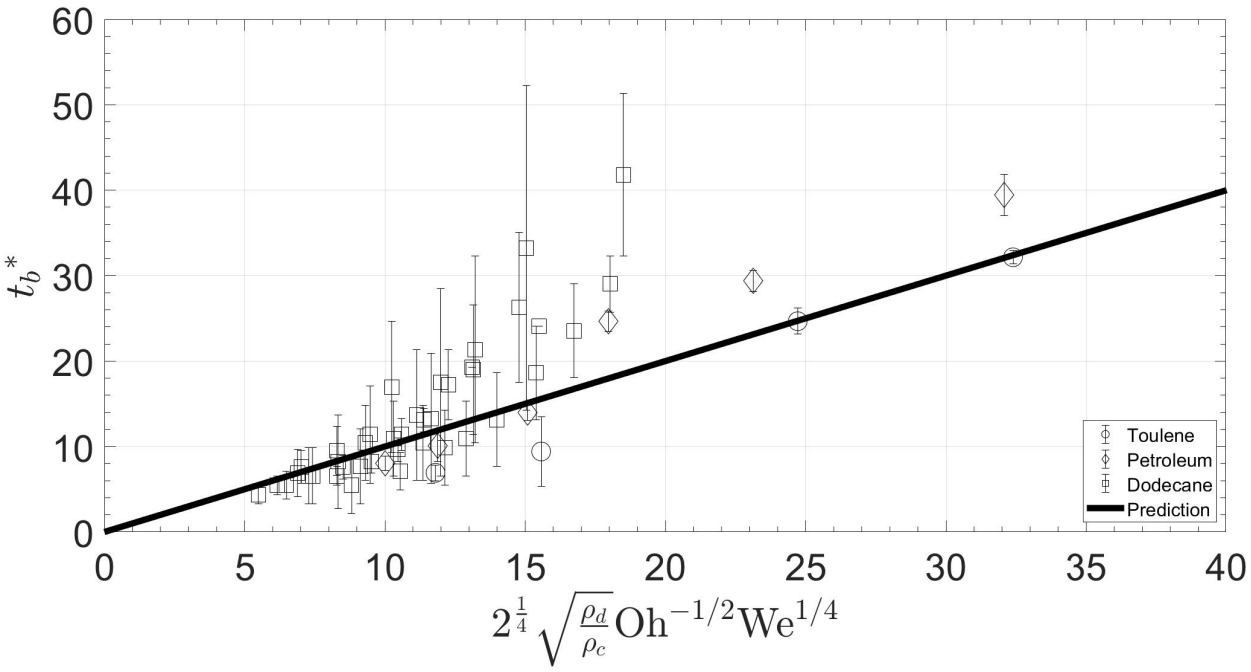

Figure 1: Dimensionless breakage time, t_b^*, as a function of dimensionless parameters for various petrochemical-water emulsions listed in Table 1. The solid line represents Eq. (16), symbols represent experimental data, and error bars depict standard errors.

One of the challenges in studying droplet breakage in heterogeneous flow fields is the limited availability of droplet breakage time data. Experimental investigations often involve varying flow conditions, such as different equipment setups, operating parameters, and fluid

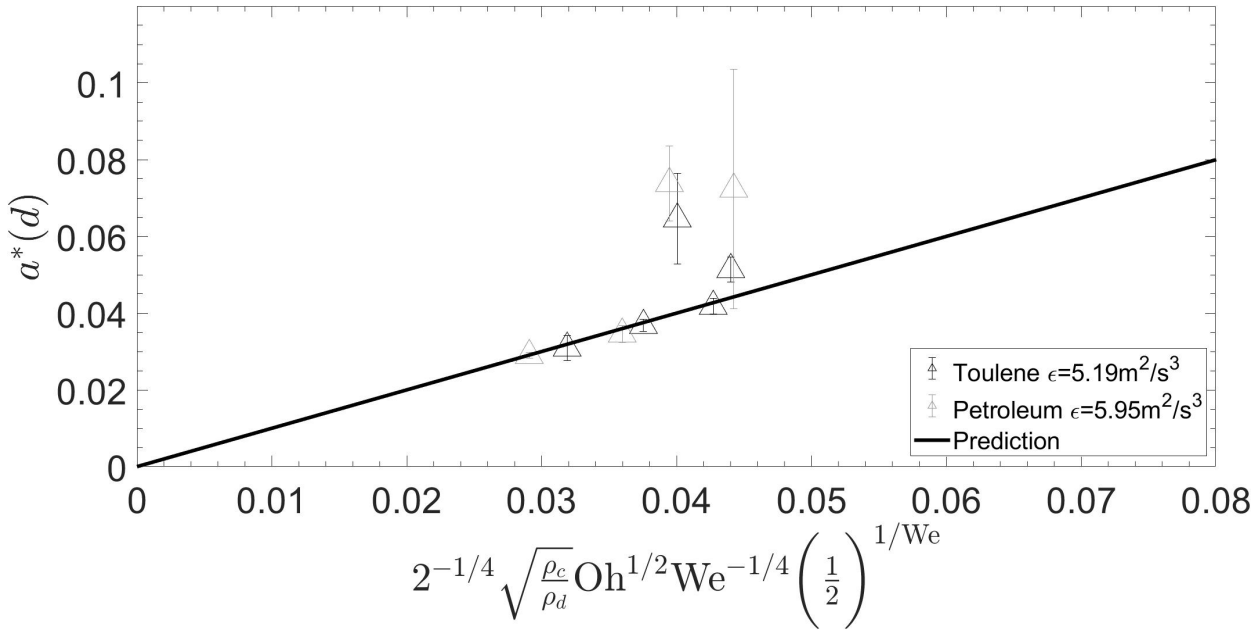

Figure 2: Dimensionless breakage rate, $a^*(d)$, as a function of parent droplet diameter for emulsions comprised of petroleum derived test fluids and water. The solid line represents Eq. (17), symbols represent experimental data, and error bars depict standard error.

properties, which make it difficult to directly compare the results obtained from different studies. However, the utilization of Eq. (16) provides a valuable approach to address this issue.

By collapsing the droplet breakage time data using Eq. (16), comparing and analyzing experimental approaches conducted under different conditions becomes easier as can be seen in Figure:2. This equation provides a dimensionless representation of the breakage time, allowing for the normalization of data across various experimental setups. Consequently, researchers can gain insights into the underlying physics of droplet breakage, independent of the specific experimental conditions.

Similarly Using Eq. (17), the dimensionless breakage rate $a^*(d)$ is plotted in Figure 2 for toulene and petroleum drops, as these were the only fluids for which data sets are available that contain information about both breakage time and breakage probability. Although it is difficult to draw firm conclusions from this plot, the predictions of Eq. (17) are consistent

with the available experimental data.

4. Experimental Method- Von Karman Flow Cell

In a study conducted by Ravichandar *et al.*. [14], a von Kármán swirling flow device was used to produce homogeneous, low-intensity turbulence suitable for carrying out droplet breakage experiments. Here, a concise summary of the experimental methodology is presented, and for a more comprehensive understanding, detailed information can be referenced in the Physics of Fluids paper [14].

The experimental configuration for droplet breakage is depicted in Fig. 3, illustrating a closed fluid supply circuit utilized for filling and emptying the test section with de-ionized water. The von Kármán box (1) is subjected to illumination through a LED tube light fixture (2) and diffuser (3) to enable high-speed video capture of droplet breakage events. The von Kármán tank was designed to have interior dimensions of 200.15 mm x 250.95 mm x 206.502 mm (10.4 liter volume) and be filled with deionized water as the continuous-phase fluid. Two syringe pumps, denoted as (4) and (5), are intricately connected to a T-junction fitting (6). De-ionized water, sourced from a reservoir, is supplied to one of the syringe pumps (4) to serve as the carrier fluid. Within the T-junction, the second syringe pump (5) is employed to regulate the flow rate of the dispersed phase, generating individual organic droplets. The manipulation of flow rates from both syringe pumps facilitates the production of droplets across a spectrum of sizes.

Each distinct oil droplet generated is then transported through flexible tubing into an injection needle situated within the von Kármán cell. Positioned opposite to the light source and orthogonal to the flow cell impellers, a high-speed camera (7) captures the dynamics of the droplet breakage phenomena.

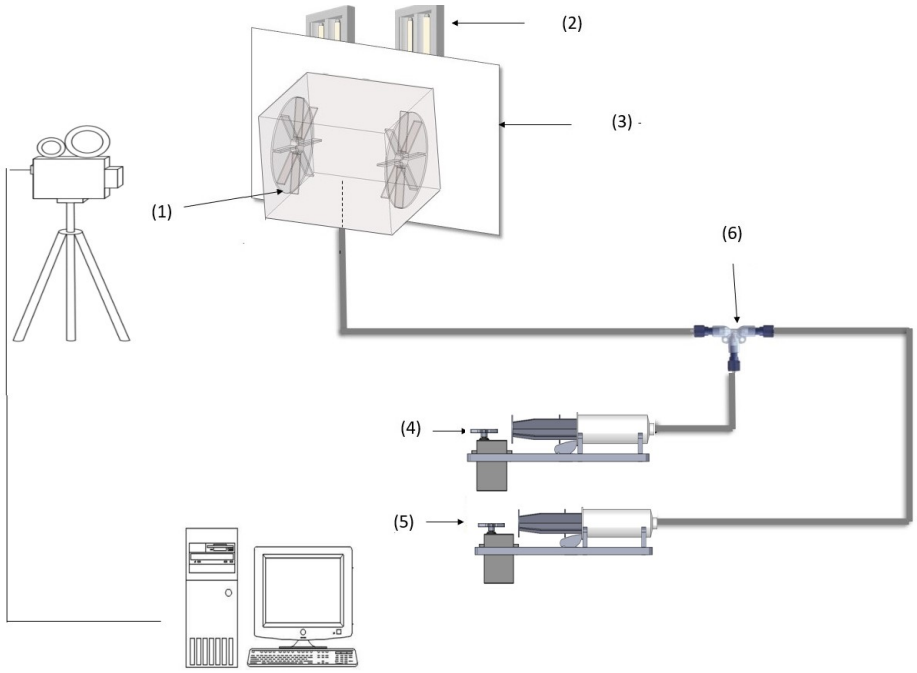

Figure 3: Schematic of the experimental setup.

4.1. Homogeneity of the Von Karman Flow Cell

Ensuring the uniformity of the breakage region within the test section is crucial, given the intentional design of the von Kármán flow cell to minimize spatial heterogeneity and establish a homogeneous isotropic turbulence region for droplet breakage. Employing 3D simulations with Ansys FLUENT 2021, utilizing the k-ε and Reynolds stress turbulence models, was integral to this process [23–26]. Rigorous grid convergence experiments were conducted, culminating in a final structured linear mesh with 817,170 nodes and almost 2.2 million elements.

Figure 5 illustrates a contour plot depicting the estimated turbulent dissipation rate and turbulent kinetic energy. Notably, the highest turbulent dissipation rate occurred at the impeller's tip, gradually decreasing towards the tank's middle, where droplets are injected. To assess homogeneity within the measurement region, a 5 cm diameter sphere at the center of the test section was considered, revealing mean turbulent dissipation rates of 0.08251 m^2s^{-3} and 0.235 m^2s^{-3} for rotation speeds of 65 and 165 rpm, respectively. Within this

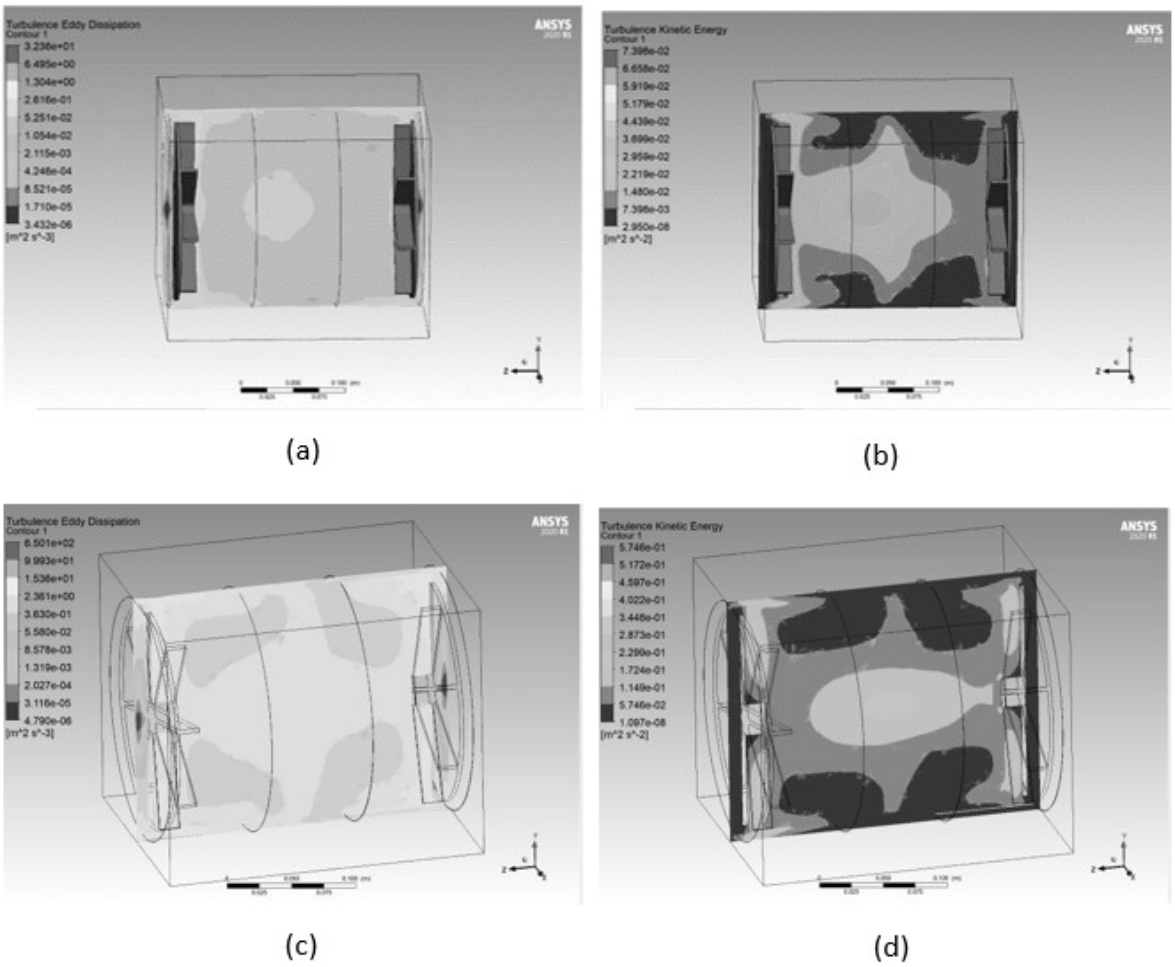

Figure 4: (a) a plot of the average ε for an impeller speed of 65 rpm, in a vertical plane perpendicular to the impellers and passing across the impeller axis of rotation. (b) a plot of the turbulent kinetic energy for an impeller speed of 65 rpm. (c) contour plot of the average ε for an impeller speed of 165 rpm. (d) contour plot of the turbulent kinetic energy for an impeller speed of 165 rpm.

sphere, local dissipation did not deviate by more than 5% from the mean dissipation rate, affirming the desired homogeneity in the turbulence field. The homogeneity of the droplet breakage region, as evidenced by the CFD results, underscores the success of the von Kármán flow cell design. Further insights into the CFD simulations that validate this homogeneity are available in previous work [13, 14], offering a deeper exploration of the computational aspects behind the observed phenomena.

4.2. Extraction of Breakage Parameters

Validation of droplet breakage models necessitates, at a minimum, the assessment of specific parameters associated with the breakage of droplets of known size. These parameters include: (1) the mean time required for a droplet to undergo breakage, (2) the fraction of droplets of a specified size that undergo breakage within a fixed observation volume, and (3) the distribution of child droplets resulting from the breakage of a parent droplet. Additionally, image sequences depicting droplets undergoing deformation, stretching, and rupture offer valuable quantitative data for refining and validating breakage models. The FASTCAM-APX RS high-speed camera, capable of capturing sequences of up to 2048 images at speeds up to 2 kHz, is employed in conjunction with custom Matlab-based software to process image sequences. This processing involves thresholding, background subtraction, binarization, and image segmentation to extract information on breakage time, breakage probability, and child droplet distribution.

The image processing procedure includes background subtraction, contrast enhancement, and binarization using Otsu's method. After binarization, droplet sizes are measured before and after breakage through the regionprops function in Matlab, allowing for the calculation of properties such as centroid coordinates, major and minor axes, and droplet radius. The ellipsoid shape of droplets is visualized using an ellipsoid function. This process is applied to each frame in the sequence. To ensure accuracy, the mass preservation of droplets is validated by determining the volumes of parent and child droplets. The volume of ellipsoidal-shaped

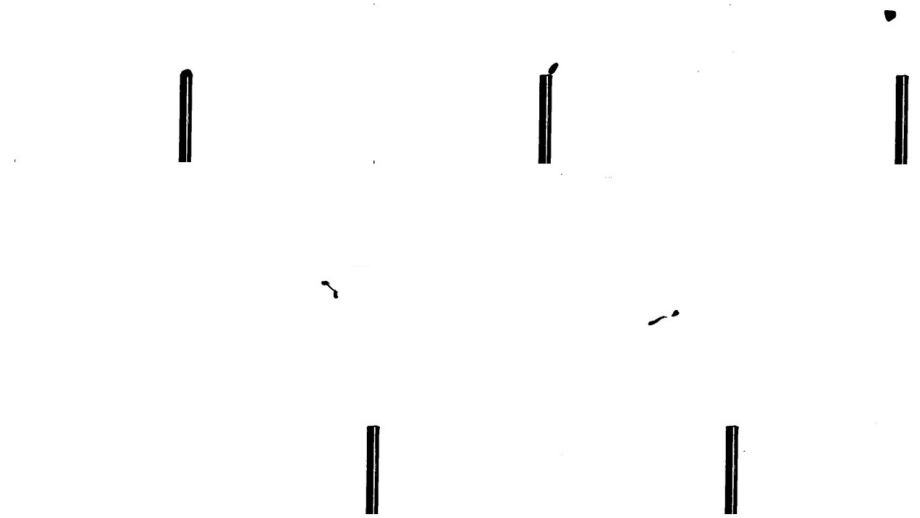

Figure 5: Sequence of oil droplet breakage captured and analyzed using custom image analysis software

droplets is estimated based on the average of their major and minor axes. The volume of child droplets is found to be approximately 90% of the volume of parent droplets, demonstrating acceptable mass conservation given the two-dimensional nature of the images. A more detailed analysis of the image processing method is highlighted in Physics of Fluids Paper [14].

4.3. Evaluation of Zero-Parameter Modified Chen Model

Vegetable oil-water systems were investigated using canola, safflower, sesame, and peanut oil as the dispersed phase, and droplet breakage time and probability were measured by analyzing thousands of droplet breakage events. Physical properties and operational parameters for these vegetable oil and water experiments are listed in Table 3. A comparison of the Weber and capillary numbers in Table 3 with those in Table 1 shows that the stabilizing internal viscous stress can be expected to play a significant role in determining the breakage time

Table 3: Vegetable oil in water fluid properties and operating parameters.

Droplet Phase	ρ **(kg/m^3)**	σ **(N/m)**	μ **(mPa·s)**	ε **(m^2/s^3)**	**We**	**Ca**
Canola Oil	915	0.018	65.9	0.083	0.21 - 4.2	0.236 - 0.428
				0.107	0.25 - 5.0	0.26 - 0.466
				0.192	0.37 - 7.3	0.31 - 0.57
				0.235	0.42 - 8.4	0.33 - 0.61
Safflower Oil	921	0.031	71.1	0.083	0.12 - 2.4	0.147 - 0.267
				0.107	0.14 - 2.9	0.160 - 0.291
Sesame Oil	946	0.011	43.3	0.083	0.34 - 6.8	0.249 - 0.453
				0.107	0.41 - 8.1	0.271 - 0.493
Peanut Oil	910	0.025	80.6	0.083	0.015 - 3.0	0.211 - 0.383
				0.235	0.031 - 6.1	0.300 - 0.543
Rapeseed Oil	915	0.032	65.9	100.0	0.9 - $5*10^7$	0.51 - 0.814
				105.0	1 -$5*10^7$	0.521 - 0.827
Silicone Oil	962	0.025	86.0	3.61	0.82 - 2.32	0.675 - 0.829

of vegetable oil droplets in water, in contrast with the petrochemical droplets considered in Section 3.1.

Table 4: Comparison of C_1 values obtained from predictions of Eqs. (27) with values obtained by regressing the Chen-modified C-T model to experimental data.

Canola Oil					
ε, m^2/s^3	$C_1 = \mathrm{Ca_{cr}}$	C_1, Regressed Average Fit	C_1, Regressed Lower Bound	C_1, Regressed Upper Bound	Percentage Error, Average Fit
0.083	0.341	0.368	0.280	0.666	7.34
0.107	0.360	0.373	0.270	0.986	3.43
0.192	0.408	0.403	0.295	0.724	1.24
0.235	0.426	0.421	0.325	0.621	1.19
Safflower Oil					
0.083	0.237	0.226	0.207	0.403	4.09
0.107	0.255	0.261	0.197	0.480	2.3
Sesame Oil					
0.083	0.767	0.829	0.586	1.894	7.48
0.107	0.802	0.882	0.565	1.887	9.07
Peanut Oil					
0.083	0.324	0.3230	0.246	0.407	0.3
0.235	0.405	0.4039	0.209	0.557	0.3
Rapeseed Oil					
100	0.933	1.0550	0.8811	1.442	11.5
105	0.944	0.9385	0.8569	1.138	0.06
Silicone Oil					
3.61	0.626	0.6523	0.53226	0.8281	4.0

Fitted values for C_1 were obtained from measurements of breakage time by using Eq. (9), and the resulting dimensionless breakage time curves are compared with the prediction of Eq. (27) in Figure 6 . The range of fitted values for C_1 is listed in Table 4, which shows that the fitted and predicted (i.e. $C_1 = \mathrm{Ca}_{cr}$) values differ on average by only 4.02%. Figure 6 show a remarkable collapse of breakage time data, which suggests that Eq. (27) may be useful

for predicting drop breakage time without need for carrying out an experimental campaign to determine fitting constants.

The modified Chen model for breakage rate, represented by Eq.(28), demonstrates good agreement with the experimental data on droplet breakage rate, as depicted in Figure7. However, some deviations are observed for canola oil droplets experiencing breakage under conditions of low turbulence dissipation rates. It is important to consider that these discrepancies can arise from the inherent variability in experimental data, particularly due to the transportation of larger droplets by larger eddies. As a result, the time required for these droplets to undergo breakage may be increased. Furthermore, these larger eddies can also contribute to the breakage process, thereby increasing the overall probability of breakage. In the experimental breakage rate plot, the breakage probability is divided by the breakage time, which leads to a significant increase in the variation of experimental data. Consequently, this variation may lead to a misalignment between the experimental data and the predictions provided by the model.

In summary, the modified Chen model demonstrates overall agreement with the experimental data on droplet breakage rate. However, discrepancies observed for canola oil droplets at low turbulence dissipation rates can be attributed to the transportation and breakage effects of larger eddies, as well as the inherent variability in the experimental data. Further investigations and refinements are necessary to address these deviations and improve the model's accuracy in predicting breakage rates under a wider range of conditions.

5. Conclusions

Simple relations were proposed for estimating the value of a fitting parameter (C_1) used in Eq. (9) to compute droplet breakage time [16, 19]. For cases in which droplet breakage is determined primarily by competition between deformative turbulent and resistive interfacial stresses, the hypothesis that $C_1 = 1$ is consistent with available experimental data. By

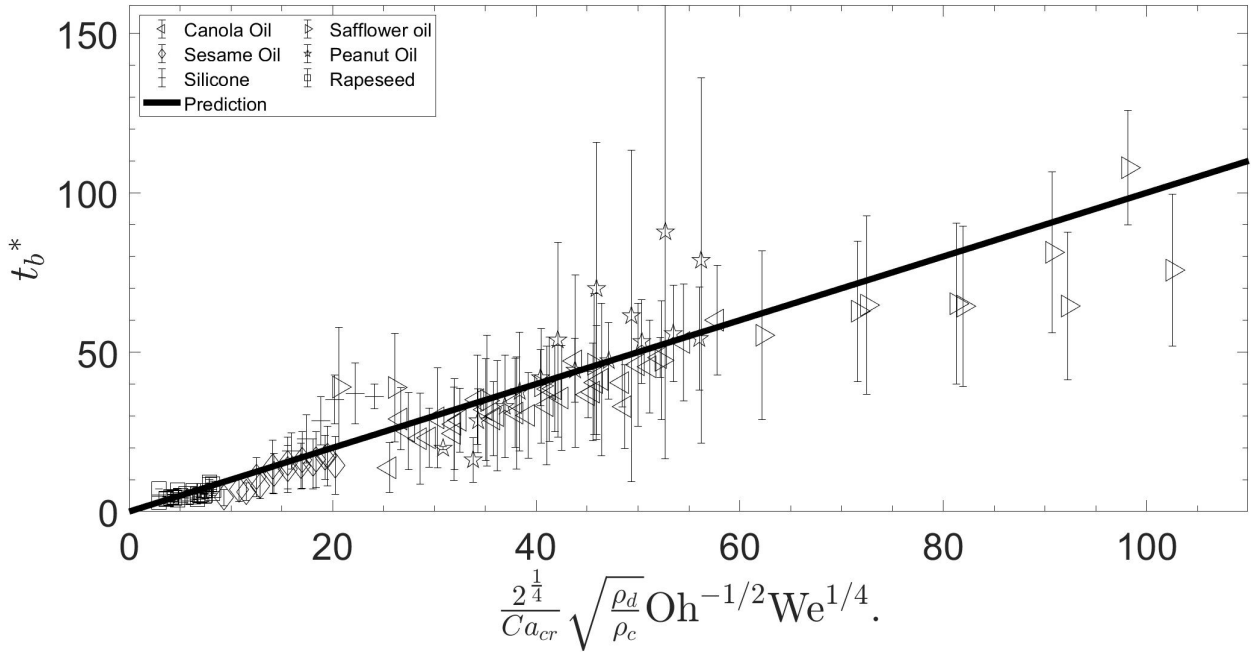

Figure 6: Dimensionless breakage time, t_b^*, as a function of dimensionless parameters for Canola Oil. The solid line represents Eq. (27), symbols represent experimental data, and error bars depict standard error.

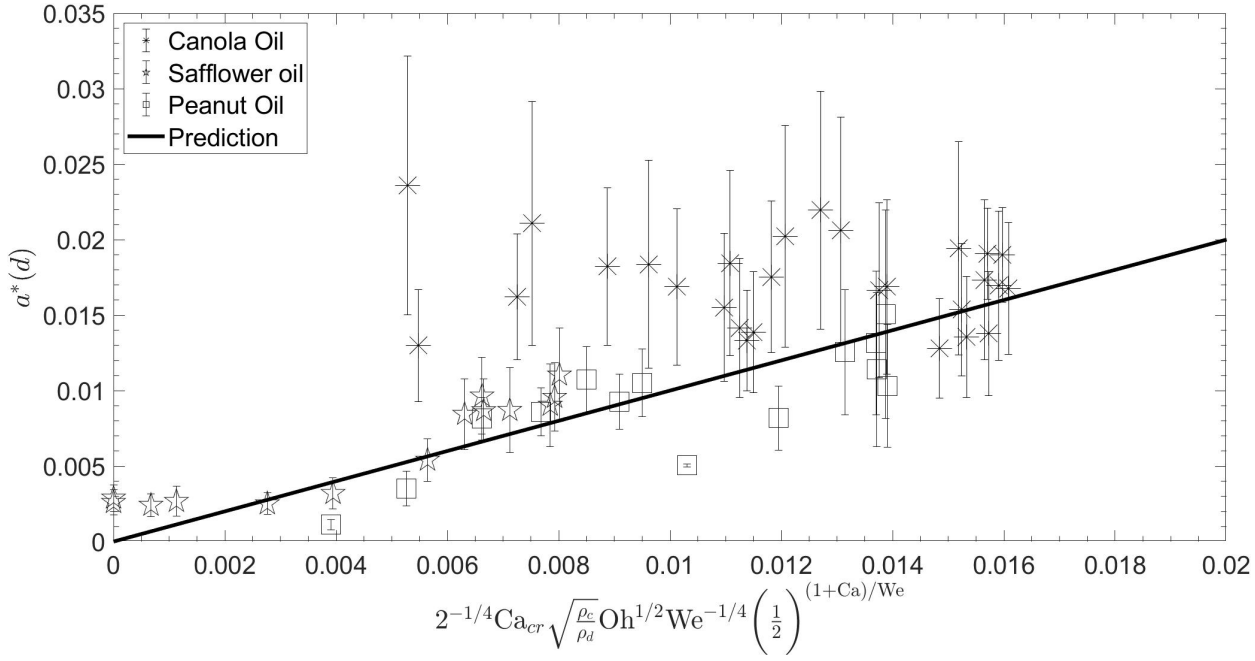

Figure 7: Dimensionless breakage rate, $a^*(d)$, plotted for vegetable oil-water emulsions listed in Table 3. The solid line represents Eq. 28. Symbols represent experimental data, and error bars depict standard error in the data.

using this value of C_1, in conjuction with a previously determined relation for a second fitting parameter associated with droplet breakage [13], a version of the well-known C-T breakage rate model that has no unknown parameters, given by Eq. (28) was constructed and compared to available breakage rate data for petroleum and toluene droplets dispersed in water.

For cases in which droplet viscosity contributes a significant portion of the cohesive stress resisting drop breakage, C_1 was assumed to be given by a critical capillary number, Ca_{cr}, associated with conditions for which droplets have a 50% chance of undergoing breakage. This critical capillary number can be computed *a priori*, and without need for carrying out experiments, by equating the disruptive turbulent deformation stress with the sum of the cohesive interfacial and internal viscous stresses. A comparison of this assumed value for C_1 with values obtained by fitting C_1 to experimental data for a variety of vegetable oil-water emulsions shows very close agreement and it is able to collapse the relevant experimental data when plotted in dimensionless coordinates. Therefore, by using $C_1 = \mathrm{Ca}_{cr}$ as well as expressions that were previously derived to replace fitting parameters related to breakage probability in the Chen model [13, 15], a predictive version of the Chen breakage model can be constructed, as shown in Eq. (28). Comparison of the resulting breakage rate predictions with experimental data shows good agreement.

The findings presented in this work hold significant implications for the design, optimization, and scale-up of equipment. The derived equations, Eqns. (17) and (28), provide a valuable tool for predicting breakage rates without relying on extensive empirical studies to determine fitting constants. This breakthrough greatly accelerates the process of equipment design and optimization, saving valuable time and resources.

However, it is important to acknowledge the limitations of this study. While the derived equations have been partially validated in this work, further experimental investigations are necessary to validate their applicability across a wider range of test fluids. This step will

enhance the reliability and robustness of the predictive models and ensure their accurate implementation in industrial settings.

The prospects of this research extend beyond its immediate applications. The approach taken in this study, which combines mathematical modeling with empirical validation, holds the potential to improve other breakage rate models as well. By incorporating similar methodologies, researchers can refine and enhance existing models, leading to more accurate predictions and a deeper understanding of breakage phenomena in various engineering processes.

In summary, this work's significance lies in the development of predictive equations, Eqns. (17) and (28), which eliminate the need for empirical studies to determine fitting constants, thereby expediting equipment design and optimization. However, further experimental validation is crucial to broaden the range of applicable fluids. Moreover, this research sets the stage for advancements in breakage rate modeling and opens avenues for improving other related models in the field.

Conflict of Interest Statement

The authors have no conflicts to disclose

Acknowledgement

This work was supported by the National Science Foundation grant CBET-2201707.

Data Availability Statement

The data that support the findings of this study are available from the corresponding author upon request.

References

[1] Eirik H. Herø, Nicolas La Forgia, Jannike Solsvik, and Hugo A. Jakobsen. Single drop breakage in turbulent flow: Statistical data analysis. *Chemical Engineering Science: X*, 8, 11 2020.

[2] C. Li, J. Miller, J. Wang, S. S. Koley, and J. Katz. Size distribution and dispersion of droplets generated by impingement of breaking waves on oil slicks. *Journal of Geophysical Research: Oceans*, 122, 2017.

[3] Stephanie Nachtigall, Daniel Zedel, and Matthias Kraume. Analysis of drop deformation dynamics in turbulent flow. *Chinese Journal of Chemical Engineering*, 24:264–277, 2 2016.

[4] D. Maggioris, A. Goulas, A. H. Alexopoulos, E. G. Chatzi, and C. Kiparissides. Prediction of particle size distribution in suspension polymerization reactors: Effect of turbulence nonhomogeneity. *Chemical Engineering Science*, 55, 2000.

[5] D.J McClements. Food emulsions and foams: Interfaces, interactions and stability, edited by e. dickinson and j.m. rodriguez, the royal society of chemistry, cambridge, 1999, pp. 390, isbn 0-85404-753-0, uk £85.00. *Colloids and Surfaces A: Physicochemical and Engineering Aspects*, 160, 1999.

[6] C. Tsouris and L. L. Tavlarides. Breakage and coalescence models for drops in turbulent dispersions. *AIChE Journal*, 40(3):395–406, 1994.

[7] M. Kostoglou. On the evolution of particle size distribution in pipe flow of dispersions undergoing breakage. *Industrial & Engineering Chemistry Research*, 45(6):2143–2145, 2006.

[8] Noureddine Lebaz, Fouad Azizi, and Nida Sheibat-Othman. Modeling droplet breakage in continuous emulsification using static mixers in the framework of the entire spectrum of turbulent energy. *Industrial & Engineering Chemistry Research*, 61(1):541–553, 2022.

[9] Guancheng Tan, Kun Qian, Shuxian Jiang, Jianqing Wang, and Jiajun Wang. Cfd-pbm investigation on droplet size distribution in a liquid–liquid stirred tank: Effect of impeller type. *Industrial & Engineering Chemistry Research*, 62(9):4109–4121, 2023.

[10] Simone Castellano, Lorenzo Carrillo, Nida Sheibat-Othman, Daniele Marchisio, Antonio Buffo, and Sophie Charton. Using the full turbulence spectrum for describing droplet coalescence and breakage in industrial liquid-liquid systems: Experiments and modeling. *Chemical Engineering Journal*, 374:1420–1432, 2019.

[11] Hean Luo and Hallvard F. Svendsen. Theoretical model for drop and bubble breakup in turbulent dispersions. *AIChE Journal*, 42(5):1225–1233, 1996.

[12] Yixiang Liao and Dirk Lucas. A literature review of theoretical models for drop and bubble breakup in turbulent dispersions. *Chemical Engineering Science*, 64(15):3389–3406, 2009.

[13] Krishnamurthy Ravichandar, R. Dennis Vigil, and Michael Olsen. Design and operation of a von karman reactor for droplet breakage experiments. *Elsevier BV*, 2023.

[14] Krishnamurthy Ravichandar, R. Dennis Vigil, Rodney O. Fox, Stephanie Nachtigall, Andreas Daiss, Michal Vonka, and Michael G. Olsen. Turbulent droplet breakage in a von kármán flow cell. *Physics of Fluids*, 34(7):073319, 2022.

[15] Zhong Chen, Jan Prüss, and Hans Joachim Warnecke. A population balance model for disperse systems: Drop size distribution in emulsion. *Chemical Engineering Science*, 53, 1998.

[16] C.A. Coulaloglou and L.L. Tavlarides. Description of interaction processes in agitated liquid-liquid dispersions. *Chemical Engineering Science*, 32:1289–1297, 1977.

[17] J. O. Hinze. Fundamentals of the hydrodynamic mechanism of splitting in dispersion processes. *AIChE Journal*, 1, 1955.

[18] AN Kolmogorov. Die energiedissipation für lokalisotrope turbulenz. In *Dokl. Akad. Nauk SSSR*, volume 32, pages 16–18, 1958.

[19] Nina Vankova, Slavka Tcholakova, Nikolai D. Denkov, Vassil D. Vulchev, and Thomas Danner. Emulsification in turbulent flow: 2. breakage rate constants. *Journal of Colloid and Interface Science*, 313(2):612–629, 2007.

[20] Krishnamurthy Ravichandar, Michael G. Olsen, and R. Dennis Vigil. Turbulent droplet breakage probability: Analysis of fitting parameters for two commonly used models. *Chemical Engineering Science*, 266:118311, 2023.

[21] Sebastian Maaß and Matthias Kraume. Determination of breakage rates using single drop experiments. *Chemical Engineering Science*, 70:146–164, 3 2012.

[22] Experimental study on drop breakup time and breakup rate with drop swarms in a stirred tank. *AIChE Journal*, 67(1):e17065, 2021.

[23] C. D. Argyropoulos and N. C. Markatos. Recent advances on the numerical modelling of turbulent flows, 2015.

[24] Hua Feng, Michael G. Olsen, Ying Liu, Rodney O. Fox, and James C. Hill. Investigation of turbulent mixing in a confined planar-jet reactor. *AIChE Journal*, 51, 2005.

[25] Ying Liu, Michael G. Olsen, and Rodney O. Fox. Turbulence in a microscale planar confined impinging-jets reactor. *Lab on a Chip*, 9, 2009.

[26] Amina Meslem, Florin Bode, Cristiana Croitoru, and Ilinca Nastase. Comparison of turbulence models in simulating jet flow from a cross-shaped orifice. *European Journal of Mechanics, B/Fluids*, 44, 2014.